# Electronic Supplementary Information

## Dynamic disulfide bond networks enable self-healable and mechanically resilient intrinsically stretchable organic solar cells

*Wenyu Yang,[a] Xuanang Luo,[a] Jiankang Liu,[a] Jingchuan Chen,[a] Xuefei Wu,[b] Zachary Fink,[b] Chuqi Shi,[c] Wenkai Zhong*[, a], Cheng Wang,[d] Lei Ying*[, a]*

[a] Institute of Polymer Optoelectronic Materials and Devices, Guangdong Basic Research Center of Excellence for Energy & Information Polymer Materials, State Key Laboratory of Luminescent Materials and Devices, South China University of Technology, Guangzhou 510640, China
E-mail: wkzhong@scut.edu.cn; msleiying@scut.edu.cn

[b] Materials Science Division, Lawrence Berkeley National Laboratory, Berkeley, CA 94720, United States

[c] Tsinghua Shenzhen International Graduate School, Tsinghua University, Shenzhen 518055, China

[d] Advanced Light Source, Lawrence Berkeley National Laboratory, Berkeley, CA 94720, United States

## Experimental Section

### Materials

All reagents and chemicals were purchased from commercial suppliers, including Aldrich, Alfa Aesar, and J&K, and used without further purification unless otherwise noted. PTzBI-oF was supplied by Dongguan VoltAmp Optoelectronics Technology Co., Ltd. PYIT and PNDIT-F3N were obtained from Solarmer Inc. (China), and PETMP was sourced from Tokyo Chemical Industry.

### Synthesis

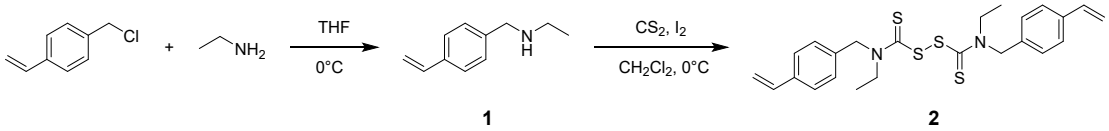


**Scheme 1.** Synthetic route of BVTD molecule (compound 2).

***Preparation of N-(4-vinylbenzyl)ethanamine (1)***

Compound 1 was prepared following a previously reported method.[1]

***Preparation of N, N'-diethyl-N, N'-bis(4-vinylbenzyl)thiuram disulfide (BVTD) (2)***

Compound 2 was synthesized according to a similar reported procedure.[2] Compound 1 (8.06 g, 50 mmol) and chloroform (25 mL) were placed in a round-bottom flask cooled in an ice bath. Carbon disulfide (1.5 mL, 25 mmol) and iodine (3.18 g, 12.5 mmol) were then added sequentially. The reaction mixture was stirred for 3 hours and subsequently washed with water. The organic phase was dried by anhydrous $Na_2SO_4$, concentrated under reduced pressure, and purified by column chromatography (silica gel) using a mixture of petroleum ether:ethyl acetate as the eluent, giving a 3.65 g transparent yellow oil. (Yield: 70%) $^1$H NMR (500 MHz, $CDCl_3$): δ = 7.39 (d, *J* = 7.9 Hz, 4H), 7.29 (d, *J* = 7.9 Hz, 4H), 6.69 (dd, *J* = 17.5, 10.9 Hz, 2H), 5.72 (d, *J* = 17.5 Hz, 2H), 5.26 (d, *J* = 10.9 Hz, 2H), 4.03 (s, 4H), 1.43 (q, *J* = 7.1 Hz, 4H), 1.26 (t, *J* = 7.1 Hz, 6H).

**Fabrication of OSC devices with rigid substrates**

The solar cell devices were fabricated with the structure ITO/PEDOT:PSS/active layer/PNDIT-F3N/Ag. ITO-patterned glass substrates were sequentially cleaned by sonication in detergent, deionized water, and isopropyl alcohol. After drying in an oven, the substrates were treated with oxygen plasma for 2 minutes and then spin-coated with PEDOT:PSS (Clevios PVP Al 4083) at 4000 rpm, achieving a thickness of ~15 nm. The PEDOT:PSS films were then annealed on a hot plate at 150 °C for 15 minutes in air. Subsequently, the substrates were moved to a nitrogen-filled glovebox. For blend films without network, PTzBI-oF and PYIT were dissolved in chloroform at concentrations of 8 mg/mL, and then PTzBI-oF and PYIT were sequentially casted. For blend films with network, PETMP and BVTD (1:2, wt:wt) were pre-dissolved in chloroform at 8 mg/mL at room temperature, and then added to the PTzBI-oF solution. The PTzBI-oF solution was spin-coated onto the PEDOT:PSS layer at 1500 rpm and thermally annealed at 100 °C for 5 minutes. The thiol-ene click based crosslinked reaction was done through 365 nm UV illumination for 5 minutes during thermal annealing. Next, the PYIT layer was spin-coated at 2000 rpm and thermally annealed at 100 °C for 5 minutes. A 1 mg/mL PNDIT-F3N methanol solution was then spin-coated on top of the active layer at 3000 rpm. Finally, a 100 nm layer of Ag was thermally evaporated onto the interface through a shadow mask in a vacuum chamber at a pressure of $3 \times 10^{-7}$ torr. The effective device area was defined as 0.05 $cm^2$, with the active area further limited to 0.032 $cm^2$ using a non-refractive mask to improve measurement accuracy.

**Fabrication of IS-OSC devices**

The IS-OCS devices were fabricated with the structure TPU/PEDOT:PSS (M-PH1000)/PEDOT:PSS (4083)/active layer/PNDIT-F3N/EGaIn@Ag. The stretchable, transparent electrode was prepared by modifying PH1000 with the addition of 5 vol% dimethyl sulfoxide, 2 vol% polyethylene glycol, 0.5 vol% FS-30, and 0.1% GOPS. The resulting solution was spin-coated onto a TPU substrate at 1500 rpm, followed by

baking at 100°C for 20 minutes. Next, PEDOT:PSS (4083) was spin-coated onto the PH1000/TPU layer at 3000 rpm and dried at 100 °C for 20 minutes. The active layers were then spin-coated using the same conditions as for the rigid OSC fabrication. Then, PNDIT-F3N (methanol solution, 1 mg/mL) was spin-coated at 3000 rpm on the active layers. Finally, a 100 nm thick Ag layer was thermally evaporated onto the interface through a shadow mask in a vacuum chamber at a pressure of $3 \times 10^{-7}$ torr. EGaIn liquid metal was then sprayed onto the Ag layer using a deposition mask, yielding the EGaIn@Ag stretchable electrodes. The effective area of the fabricated device was defined as 0.04 (0.2 × 0.2) $cm^2$.

**OSC device characterizations**

*J-V* curves were measured using a Keithley 2400 source meter with illumination (100 mW $cm^{-2}$) provided by an AM 1.5G solar simulator (SS-F5-3A, Enlitech) in a nitrogen-filled glovebox. Devices were tested using a mask to redefine the active layer area to 0.032 $cm^2$.

*J-V* curves were measured with a Keithley 2400 source meter under illumination (100 mW $cm^{-2}$) provided by an AM 1.5G solar simulator (SS-F5-3A, Enlitech) in a nitrogen-filled glovebox. EQE spectra were measured using an EQE measurement system (QE-R3011, Enlitech), with the light intensity at each wavelength calibrated using a standard single-crystal Si solar cell before the test.

Mobilities of thin films were measured using hole-only and electron-only devices with the following structures: ITO/PEDOT:PSS/active layer/$MoO_3$/Ag for hole mobility and ITO/ZnO/active layer/PNDIT-F3N/Ag for electron mobility. The dark *J-V* curves were recorded using a Keithley 2400 source meter. The mobilities were extracted using the space-charge-limited current (SCLC) method, based on the Mott-Gurney equation: $J = 9\varepsilon_r\varepsilon_0\mu V^2/8L^3$, where $J$ is the current density, $\varepsilon_r$ is the relative dielectric constant of the active layer, $\varepsilon_0$ is the vacuum permittivity, $\mu$ is the mobility, $V$ is the effective voltage, and $L$ is the thickness of active layer.

The photo-CELIV, dark capacitance-voltage (*C-V*) and capacitance-frequency (*C-F*) curves of devices were measured using the PAIOS platform (FLUXiM, Switzerland).

**General characterizations**

$^1$H nuclear magnetic resonance (NMR) spectrum was measured on a Bruker AV-400 MHz spectrometer with tetramethyl silane (TMS) as the internal reference. UV-vis-NIR absorption spectra of thin films were measured by a SHIMADZU UV-3600 spectrophotometer. The films were prepared by spin-coating their solutions onto quartz substrates. X-ray photoelectron spectroscopy (XPS) was determined by British Kratos X-ray photoelectron spectroscopy for element analysis. The films were spin-coated on ITO substrates. Time-of-flight secondary ion mass spectrometry (TOF-SIMS) was conducted using a Nano TOF II instrument (ULVAC PHI, Japan). A $Bi_2^{3+}$ cluster primary-ion gun operating at 30 kV was employed for analysis, with a GCIB beam (5 keV, 5 nA) used for sputtering at a rate of 0.2 nm/s for depth profiling. The analysis was carried out over a 100 $\mu$m × 100 $\mu$m area, while sputtering covered a 300 $\mu$m × 300 $\mu$m area. Atomic force microscopy (AFM) images were obtained using a NanoScope NS3A system (Digital Instruments). AFM-infrared (AFM-IR) spectroscopy was performed using an Anasys nanoIR3 system (Bruker).

Grazing incidence wide angle X-ray scattering (GIWAXS) was performed on a Xenocs Xeuss 2.0 system equipped with an Excillum MetalJet-D2 X-ray source, operated at 70.0 kV and 2.8570 mA. The X-ray wavelength was 1.341 Å. PTzBI-oF/PYIT thin films were spin-coated onto PEDOT:PSS-coated silicon wafers under the same conditions used for OSC device fabrication. The X-ray beam was incident at an angle of 0.20° to probe the bulk film structure. The sample-to-detector distance was ~210 mm, and the scattering patterns were collected using a DECTRIS PILATUS3 R 1M area detector. Data processing and analysis were carried out using the Igor Pro–based Nika software package. Resonant soft X-ray scattering (RSoXS) was performed at beamline 11.0.1.2 of the Advanced Light Source (ALS), Lawrence Berkeley National Laboratory (LBNL). Films were spin-coated onto PEDOT:PSS/silicon wafer

substrates. The films were floated on deionized water by dissolving the PEDOT:PSS layer and then transferred onto silicon nitride windows for scattering experiments in transmission mode. Scattering images were captured using a Princeton Instruments PI-MTE CCD camera with a pixel size of 0.027 mm × 0.027 mm. Data reduction was performed using the Igor-based Nika package.[3]

**Stress-strain (σ-ε) curves of thin films**

Tensile tests were performed by a free-standing method, as reported previously.[4] The active layer solution was spin-coated onto a PEDOT:PSS-coated glass substrate. Sequential post-treatments were same as the OSC device fabrication. The sample was then placed on deionized water. As the PEDOT:PSS dissolves in water, the active layer floats on the surface. Then, the clamps of a tensile stage, equipped with frosted aluminum blocks, were adjusted to carefully capture the floating film through van der Waals forces. The deionized water was then gradually removed, leaving a free-standing active layer film on the tensile stage. The film was stretched at a speed of 0.03 mm/min. The stress (σ) and strain (ε) were calculated using the following equations:

$$Stress = F / (A \times B)$$

$$Strain = \Delta l / l_0$$

where $F$ is the applied force recorded by a highly sensitive force sensor, $A$ is the width of the film (10-12 mm), $B$ is the thickness of the film, $\Delta l$ is the elongation of the film, and $l_0$ is the initial distance between the clamps.

**Density function theory (DFT) and molecular dynamics (MD) simulation**

Molecular conformations were optimized using the Gaussian 16 software at the B3LYP-D3/6-31G** and PM6-D3 levels to obtain bimolecular geometries. Interactions were subsequently calculated at the B3LYP-D3/TZVP level. The results were analyzed and visualized using the Multiwfn[5] and VMD[6] software packages.

Molecular dynamics (MD) simulations were conducted using the DFT-optimized conformations to construct amorphous cells according to the following protocol: each

simulation cell contained three donor decamers, five acceptor tetramers, and 0/4 wt%/8 wt% of BVTD crosslinked networks. The initial density of the system was set to 0.5 g $cm^{-3}$. After energy minimization, the systems were subjected to a stress-strain procedure using the Forcite module, with applied stress increasing sequentially from 0 to 0.1, 0.5, 1.0, and 1.5 GPa. Final snapshots were collected under 1.5 GPa stress. A representative PYIT molecule was highlighted in red to evaluate the molecular mobility.

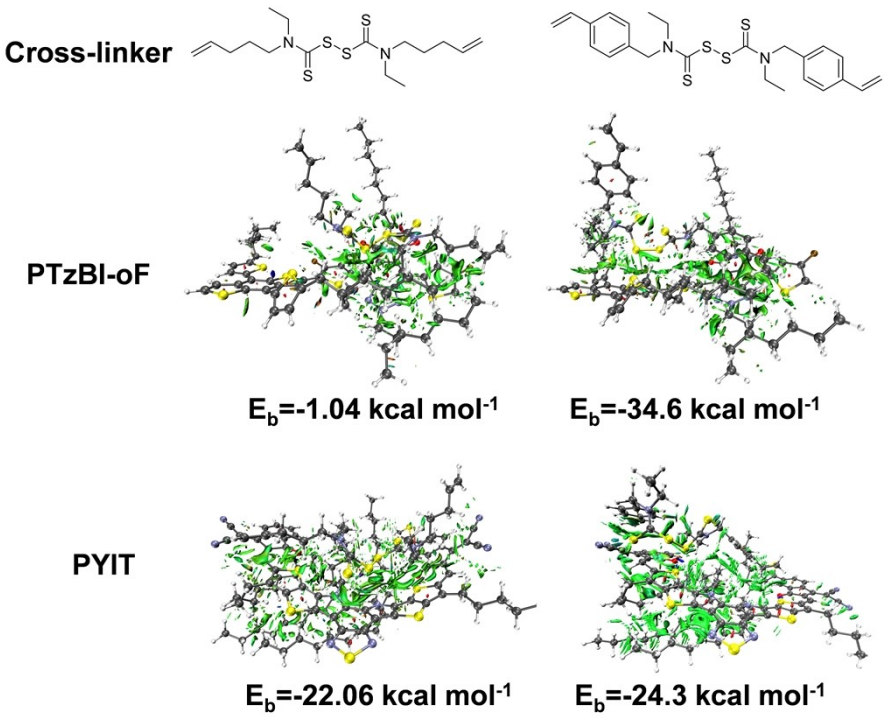


**Fig. S1** Calculated binding energies ($E_b$) between cross-linker molecules (without or with phenyl groups) and conjugated polymer fragments (PTzBI-oF or PYIT).

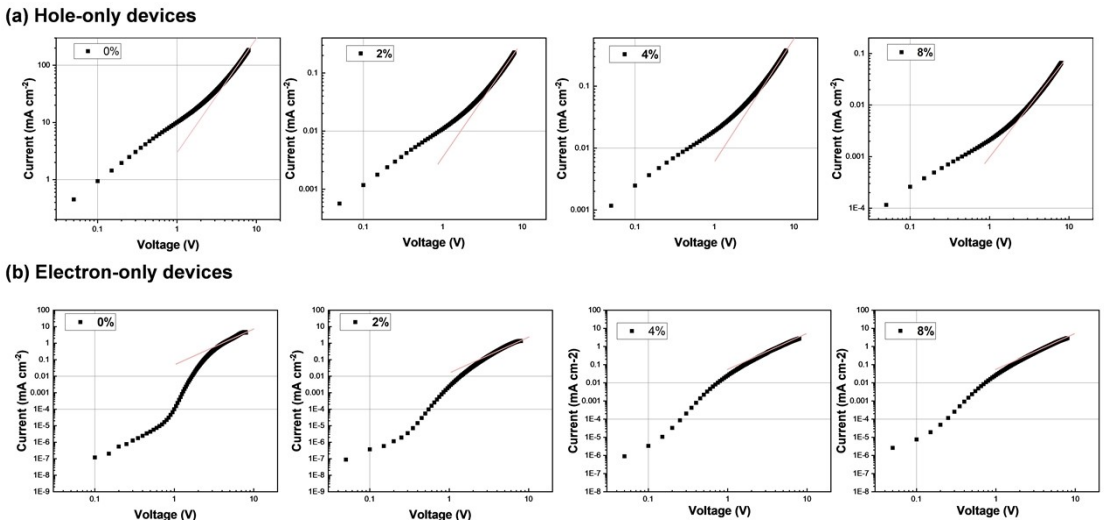


**Fig. S2** The *J-V* curves of (a) hole-only devices and (b) electron-only devices based on (PTzBI-oF+network)/PYIT, where the network was prepared with varying BVTD ratios (0%, 2%, 4%, and 8%). The red lines indicate the SCLC regions used for the calculation of mobilities.

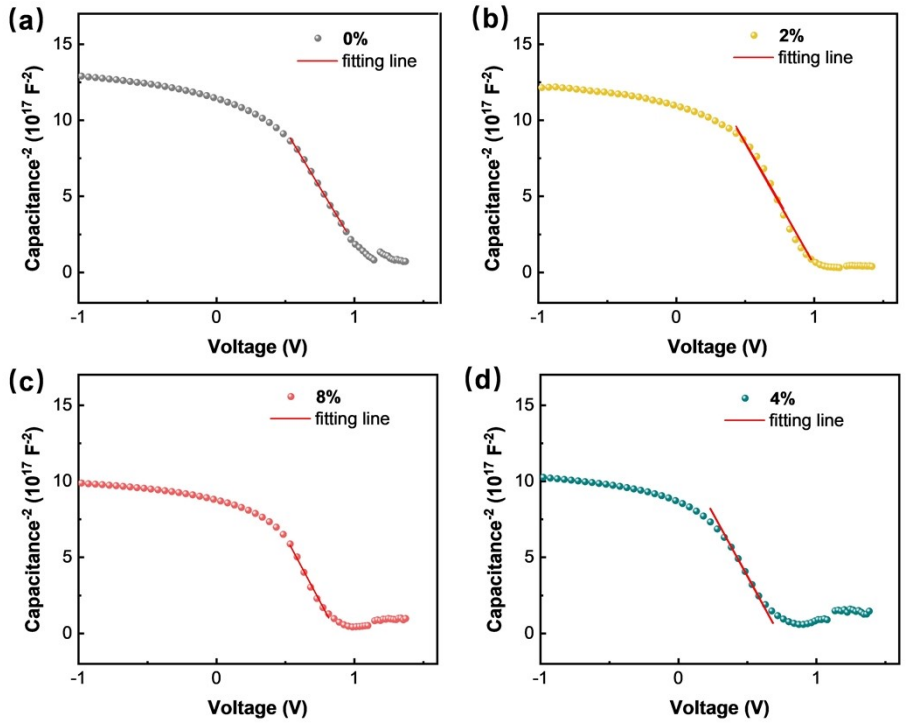


**Fig. S3** $1/C^2$-$V$ plot of OSCs fabricated with varying BVTD ratios and the results of the fitting line in the linear region.

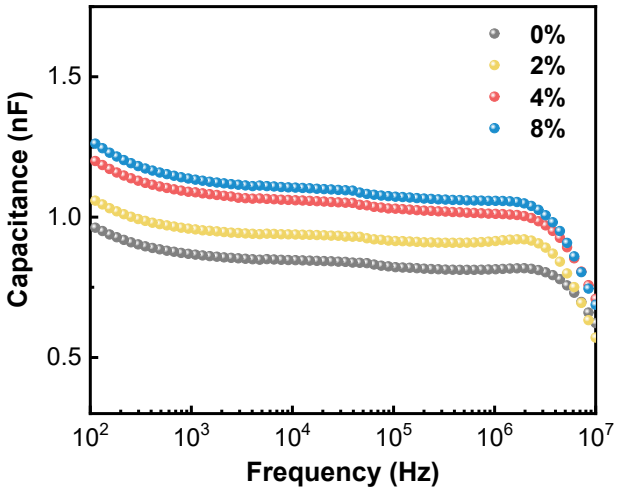


**Fig. S4** *C*-*F* characteristics of OSCs fabricated with varying BVTD ratios.

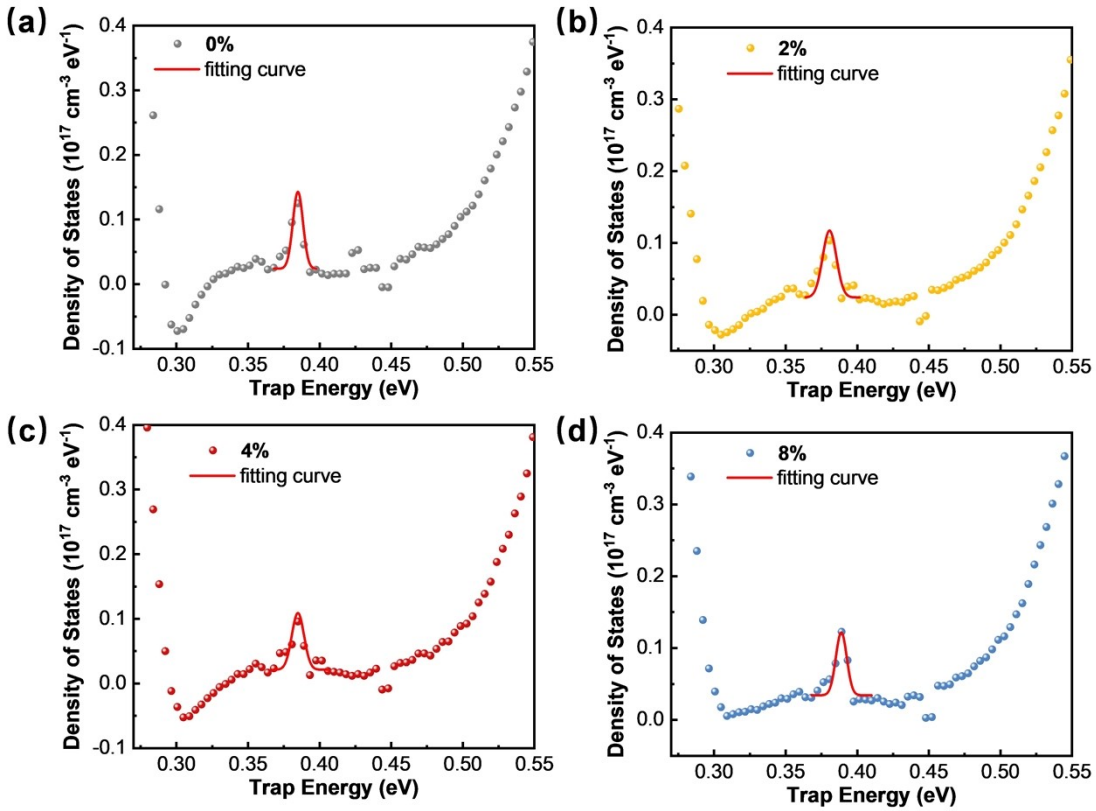


**Fig. S5** tDOS-$E_\omega$ curves of OSCs fabricated with varying BVTD ratios and the fitting results.

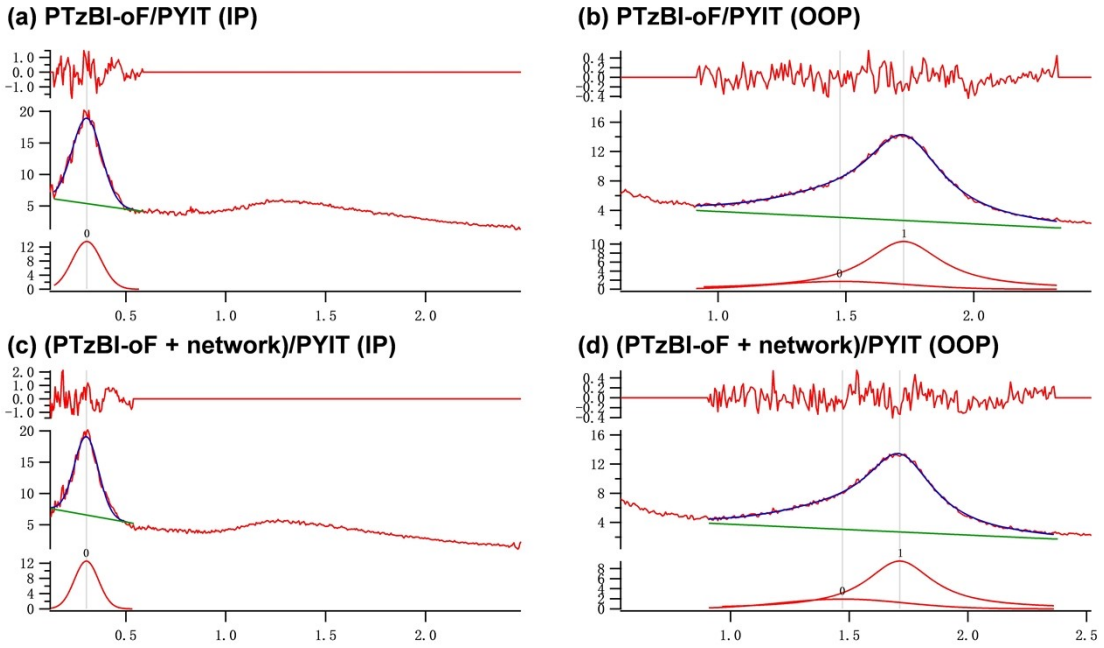


**Fig. S6** Peak-fitting for GIWAXS I-q curves in the IP and OOP directions of (a,b) PTzBI-oF/PYIT, (c,d) (PTzBI-oF + network)/PYIT films.

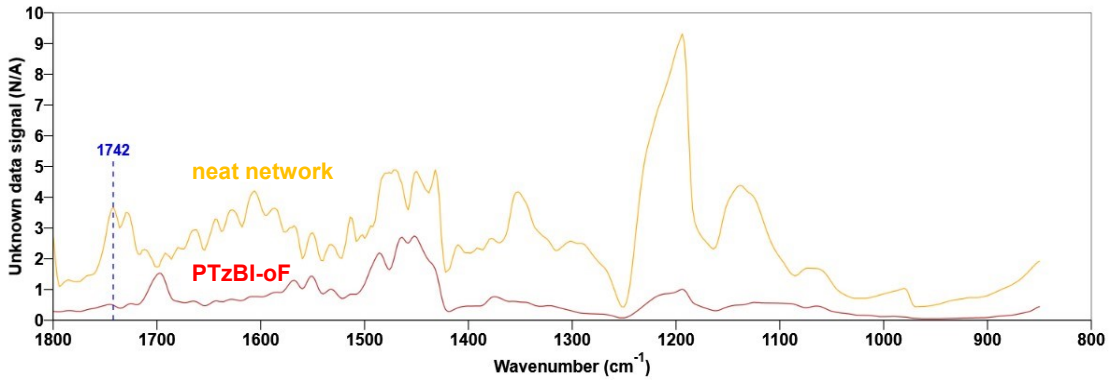


**Fig. S7** IR spectra of PTzBI-oF and the network (BVTD:PETMP = 2:1) thin film, where the wavenumber of 1742 $cm^{-1}$ can be used to highlight the network by AFM-IR.

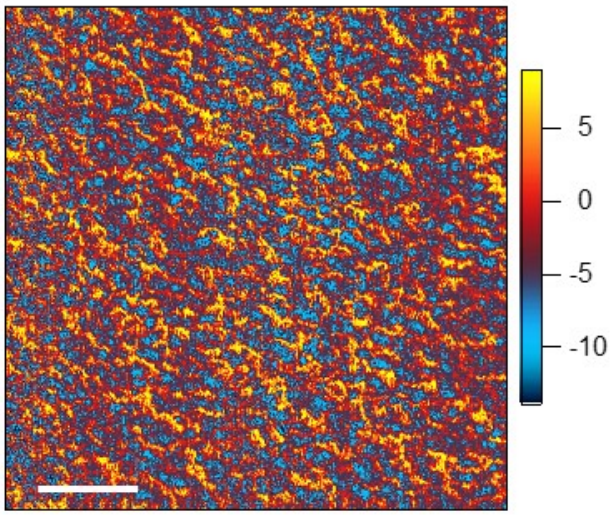


**Fig. S8** AFM-IR images of PTzBI-oF + network (8% BVTD) thin film probed at 1742 $cm^{-1}$, while scale bar in the image represents 0.25 $\mu$m, and the color bar indicates the IR amplitude.

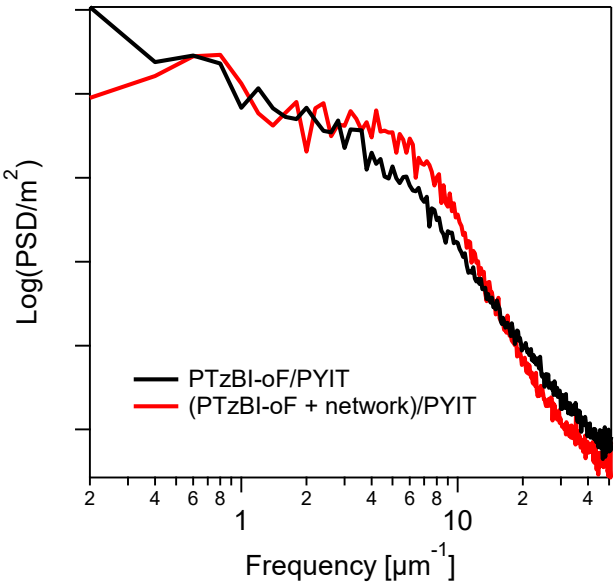


**Fig. S9** Power spectral density (PSD) analysis for the AFM height images of PTzBI-oF/PYIT and (PTzBI-oF + network)/PYIT blend films, where the network was prepared with 4 wt% BVTD relative to the PTzBI-oF.

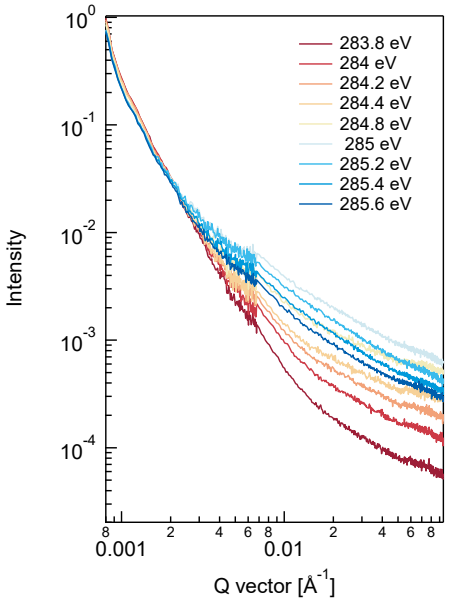


**Fig. S10** RSoXS *I-q* curves of PTzBI-oF + network (4% BVTD) thin film at different energies at C K-edge.

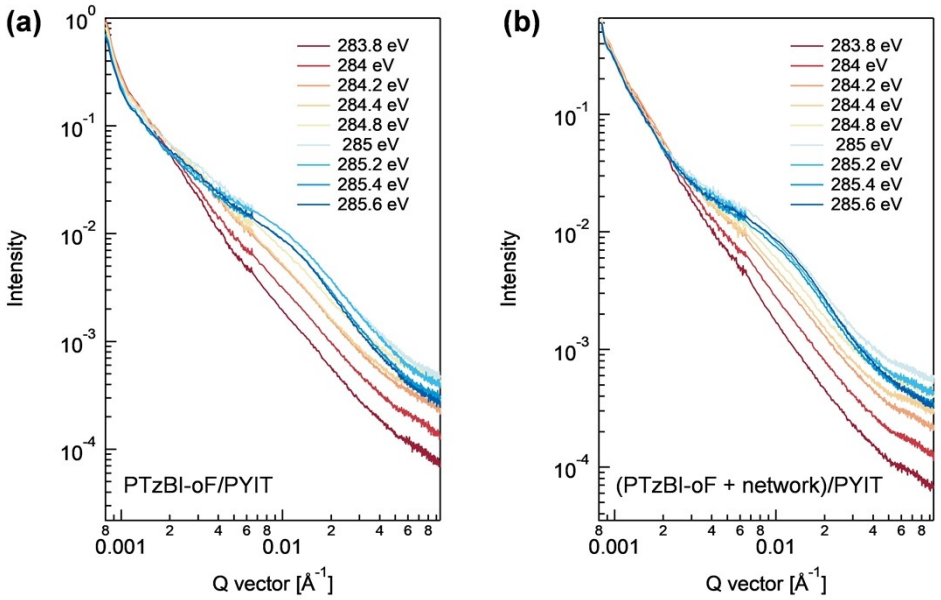


**Fig. S11** RSoXS *I-q* curves of PTzBI-oF/PYIT, (PTzBI-oF + network)/PYIT blend thin film at different energies at C K-edge. The network was prepared with 4 wt% BVTD relative to the PTzBI-oF.

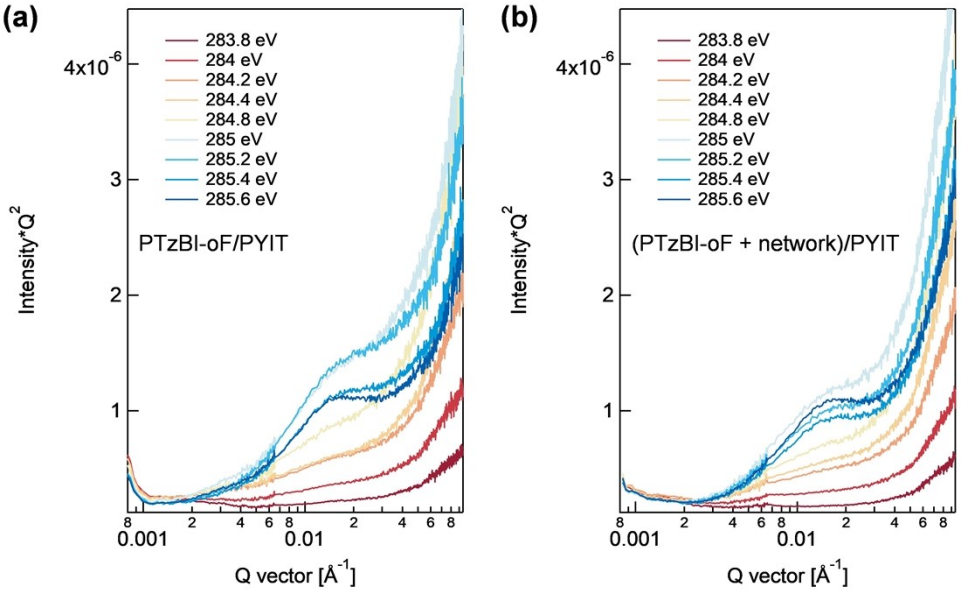


**Fig. S12** RSoXS $Iq^2$-$q$ curves of PTzBI-oF/PYIT, (PTzBI-oF + network)/PYIT blend thin film at different energies at C K-edge. The network was prepared with 4 wt% BVTD relative to the PTzBI-oF.

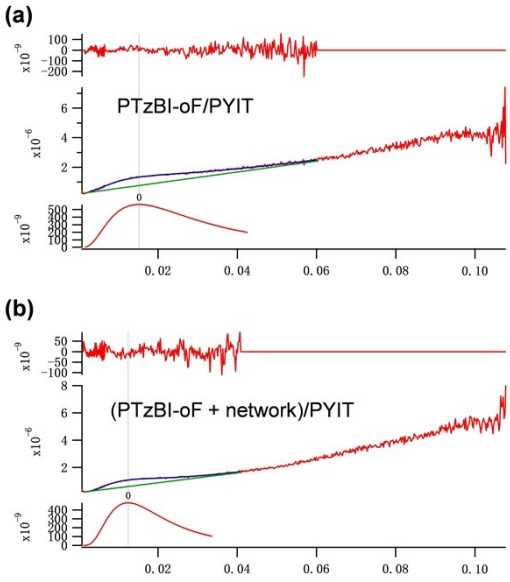


**Fig. S13** Peak-fitting for RSoXS $Iq^2$-$q$ curves with log-normal functions.

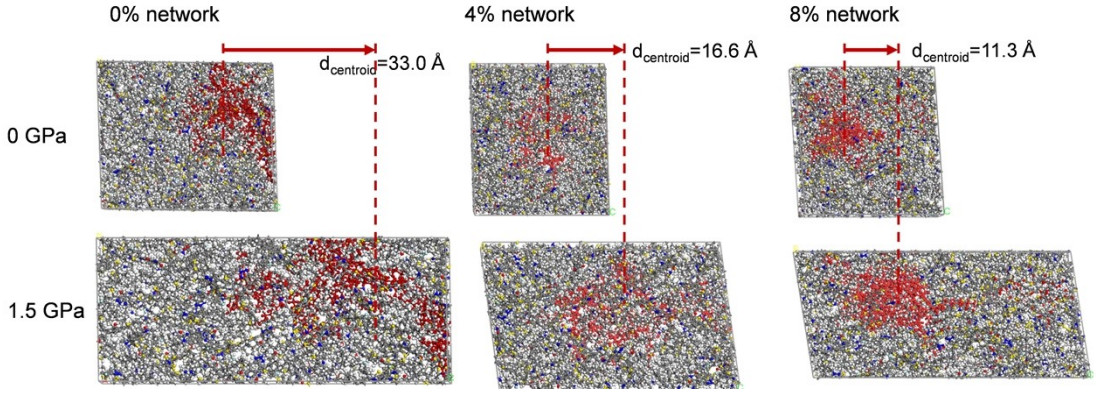


**Fig. S14** Snapshots of D/A blended cells with different network densities prepared by varying the BVTD ratio (0%, 4%, and 8%) under stress-strain molecular dynamics simulation (with the displacement of the centroid of a specific PYIT tetramers marked in red).

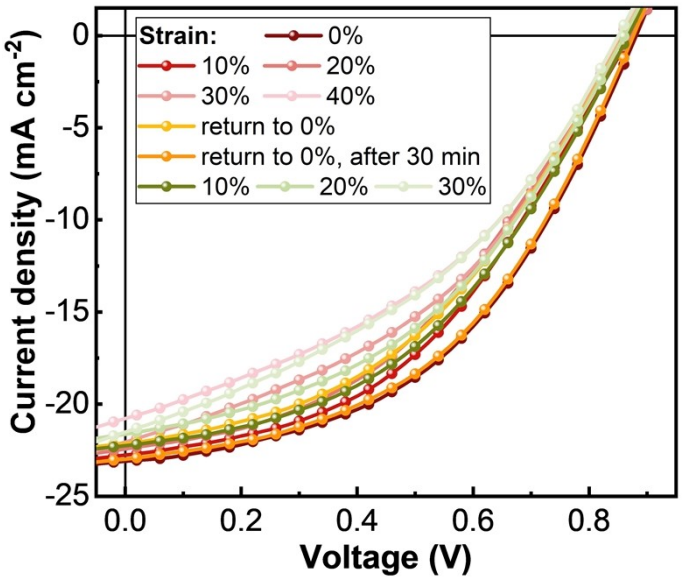


**Fig. S15** *J-V* curves of IS-OSC devices of (PTzBI-oF + network)/PYIT blend films under various strains. The network was prepared with 8 wt% BVTD relative to PTzBI-oF.

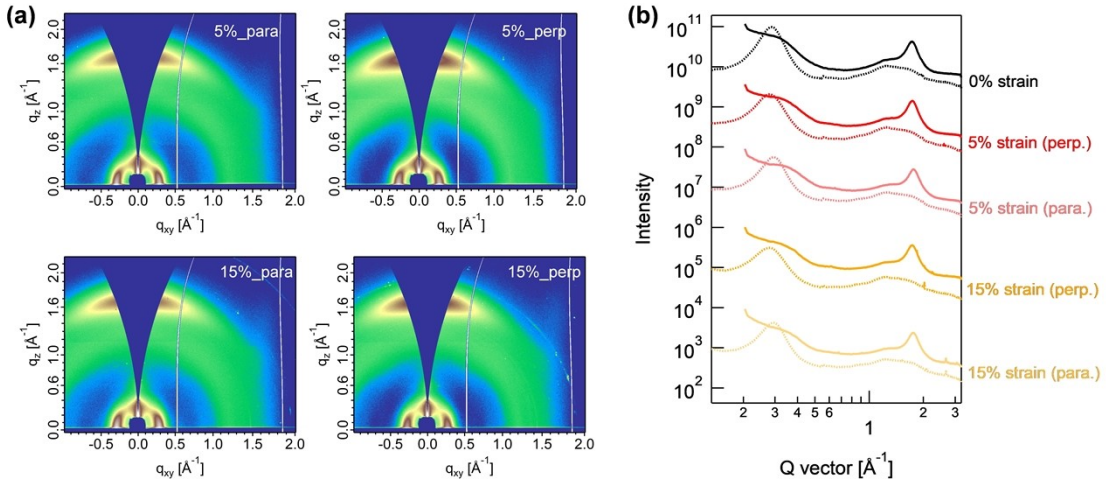


**Fig. S16** GIWAXS (a) 2D images and (b) *I-q* curves of (PTzBI-oF + network)/PYIT blend films under various strains. The network was prepared with 4 wt% BVTD relative to PTzBI-oF. GIWAXS was performed with X-ray beam perpendicular (perp.) and parallel (para.) to the strain directions.

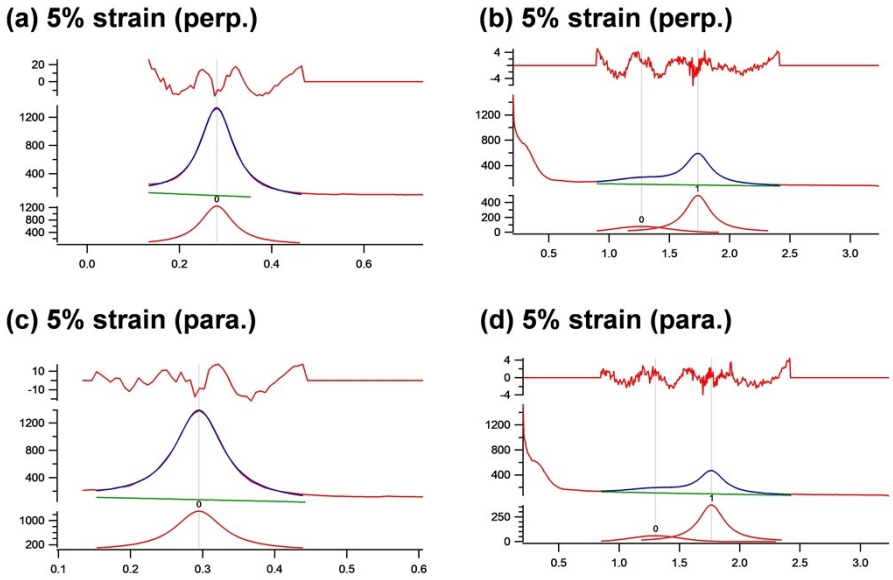


**Fig. S17** Peak-fitting for GIWAXS *I-q* curves in the (a,c) IP and (b,d) OOP directions of the PTzBI-oF + network blend films under 5% strain.

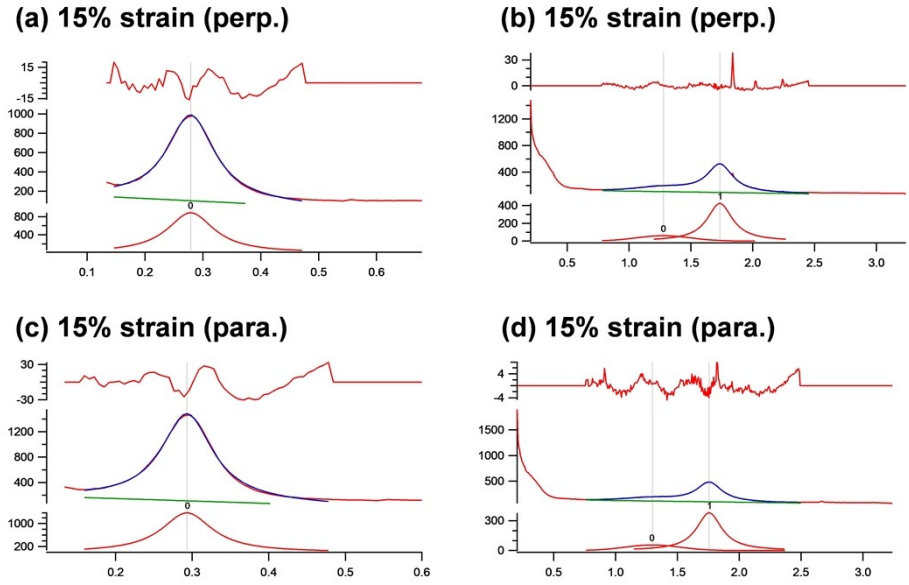


**Fig. S18** Peak-fitting for GIWAXS *I-q* curves in the (a,c) IP and (b,d) OOP directions of the PTzBI-oF + network blend films under 15% strain.

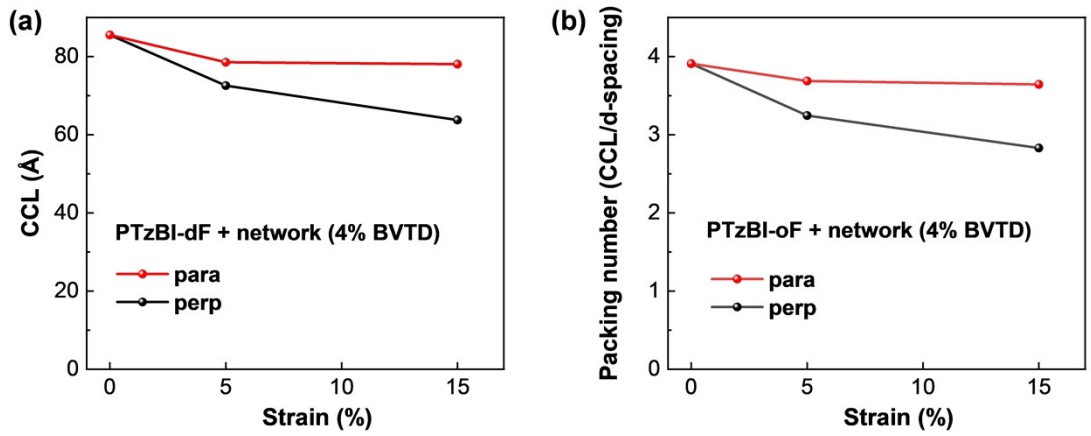


**Fig. S19** (a) CCLs and (b) packing numbers (=CCL/d-spacing) of (PTzBI-oF + network)/PYIT blend films under various strains. The network was prepared with 4 wt% BVTD relative to PTzBI-oF. GIWAXS was performed with X-ray beam perpendicular (perp.) and parallel (para.) to the strain directions.

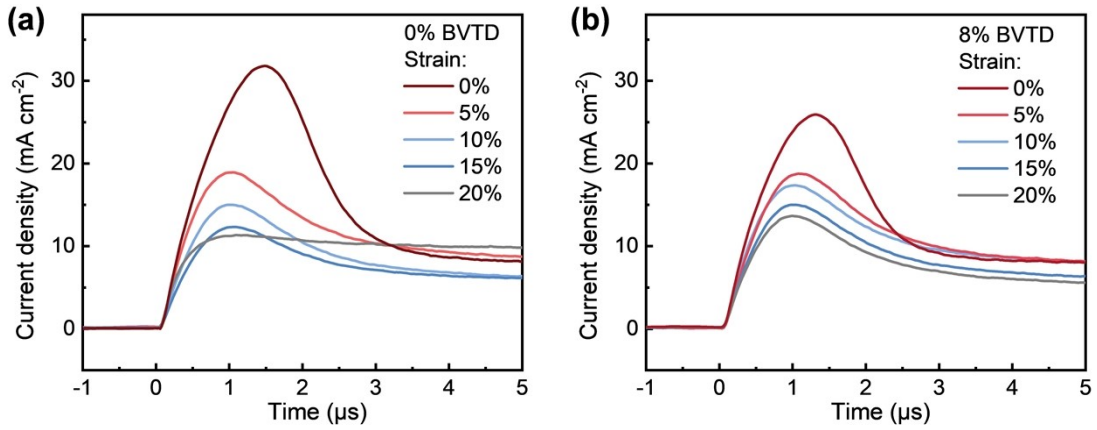


**Fig. S20** Photo-CELIV characteristics of IS-OSC devices under various strains: (a) pristine PTzBI-oF/PYIT device; (b) 8%-BVTD network based device.

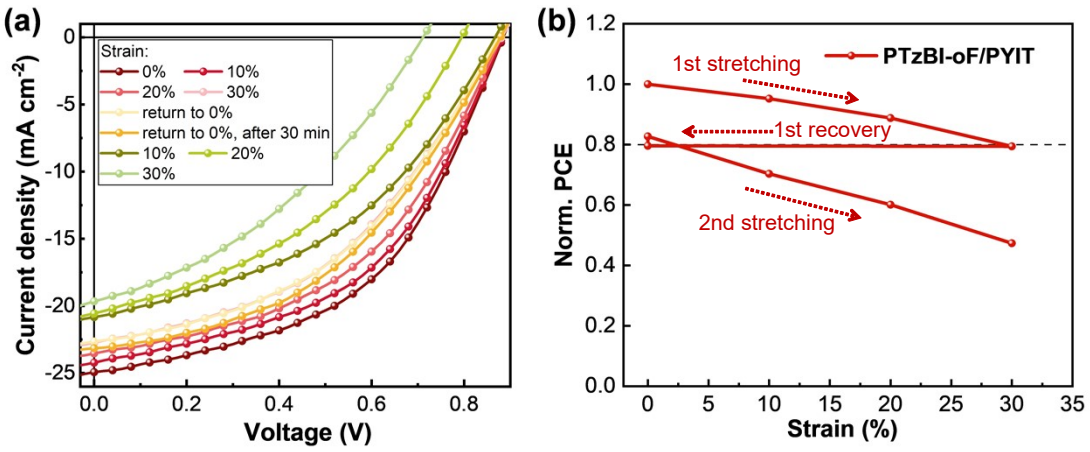


**Fig. S21** (a) *J-V* curves and (b) normalized PCE changes of IS-OSC devices of PTzBI-oF/PYIT blend films under various strains.

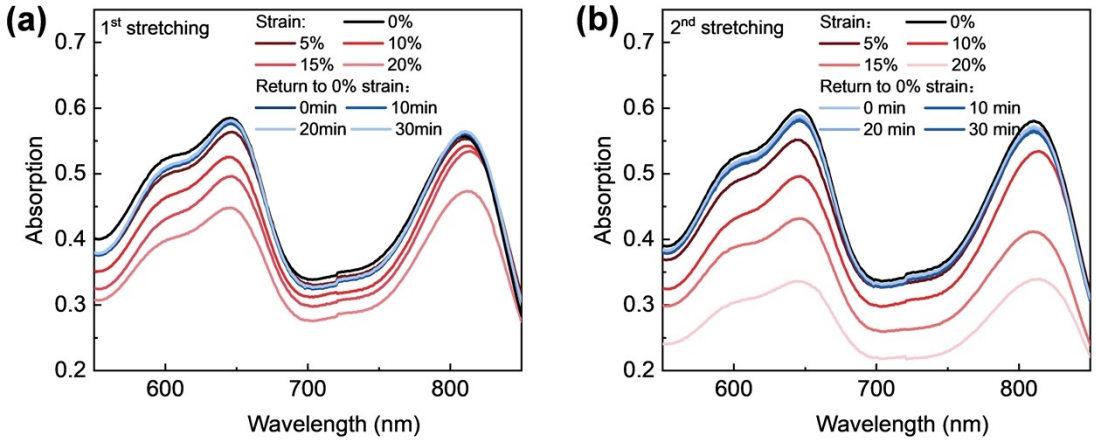


**Fig. S22** *In situ* UV-vis-NIR spectra of PTzBI-oF/PYIT thin film prepared with 8% BVTD: (a) 1st stretching-recovery cycle; (b) 2nd stretching-recovery cycle.

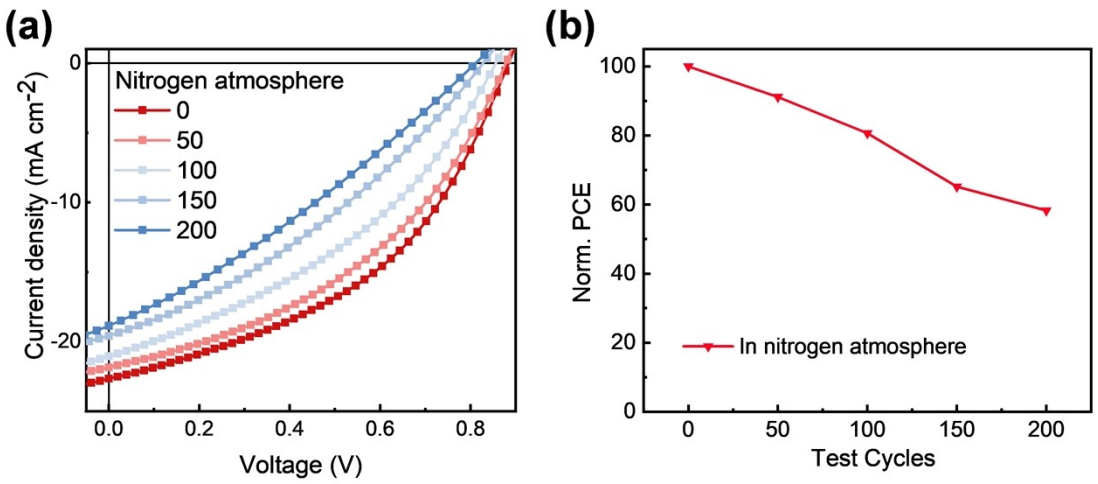


**Fig. S23** (a) *J-V* curves and (b) corresponding normalized PCE as function of test cycles of IS-OSC devices prepared with 8% BVTD. The stretching-releasing cycles of 20% strain were performed in a nitrogen-filled glove box (25 °C, $O_2$ < 5 ppm, $H_2O$ < 0.01 ppm).

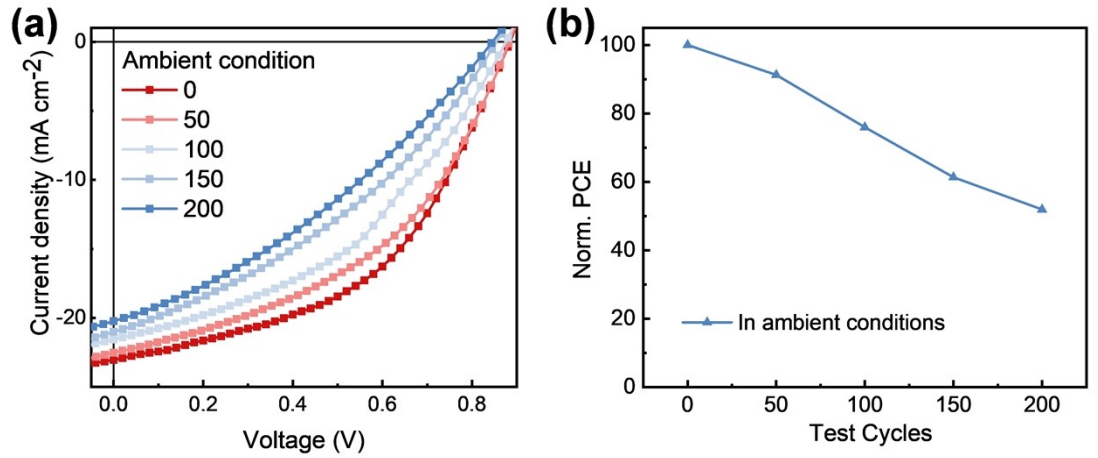


**Fig. S24** (a) *J-V* curves and (b) corresponding normalized PCE as function of test cycles of IS-OSC devices prepared with 8% BVTD. The stretching-releasing cycles of 20% strain were performed under ambient conditions (25 °C, ~40% RH, atmospheric oxygen).

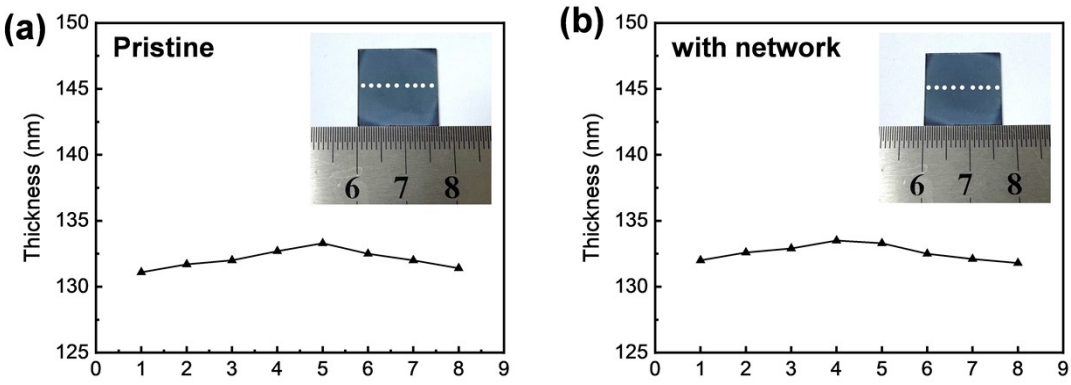


**Fig. S25** Thickness distribution measured at multiple positions across PTzBI-oF/PYIT thin films: (a) pristine film; (b) film incorporating a self-healable network with 8% BVTD. White dots in the insets indicate the locations of profilometer measurements.

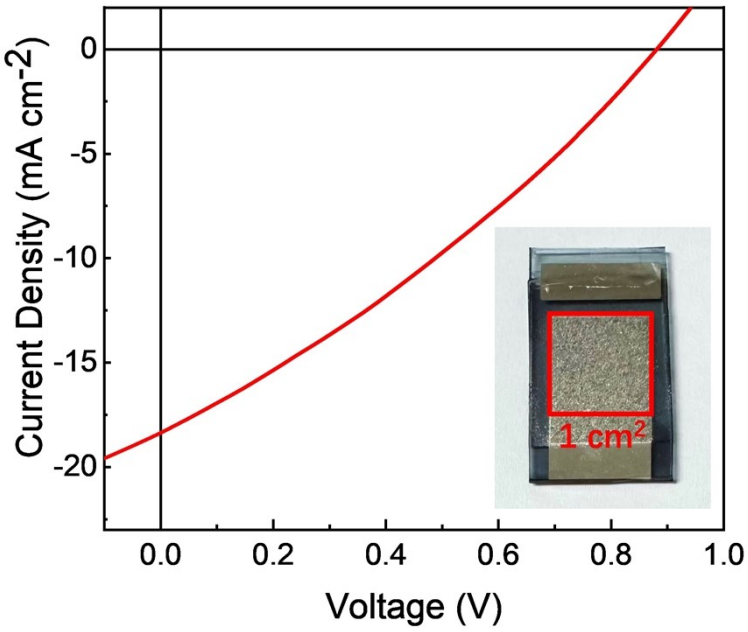


**Fig. S26** The *J*-*V* curve of the 1-cm$^2$ IS-OSC device and the image of the device (insert).

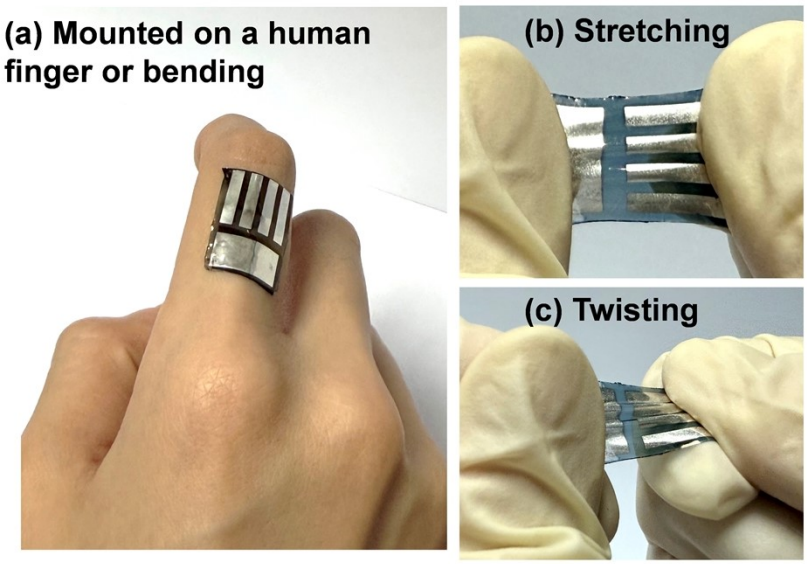


**Fig. S27** Visual demonstrations of IS-OSC devices under realistic wearable conditions: (a) mounted on a human finger or bending; (b) stretching; (c) bending.

**Table S1.** Mechanisms and healing conditions for different dynamic systems.

| Dynamic systems | Diels-Alder adducts | Disulfide exchange | Imine bonds |
|---|---|---|---|
| Mechanism | Thermally-reversible [4+2] cycloaddition between a conjugated diene and a dienophile, breaking and reforming two C–C bonds. | Reversible thiol–disulfide interchange on an S–S bond | Hydrolysis of imine bonds (C=N) to form amines and aldehydes, followed by condensation |
| Healing condition | thermal treatment at 100-150 $^{o}$C for bond dissociation, followed by a cooling process for re-bonding External heating | Disulfide bonds can react reversibly at low heat or even room temperature | Dynamic covalent bonding dependent on environmental pH and humidity |
| References | 7-8 | 9-10 | 11,12 |

**Table S2.** The hole and electron mobilities of (PTzBI-oF + network)/PYIT blend films measured by SCLC method. The self-healable network was prepared with varying BVTD ratios.

| BVTD ratio (%) | $\mu_h$ ($cm^2 V^{-1} s^{-1}$) | $\mu_e$ ($cm^2 V^{-1} s^{-1}$) |
|---|---|---|
| 0 | $1.44\times10^{-4}$ | $2.31\times10^{-4}$ |
| 2 | $1.02\times10^{-4}$ | $1.99\times10^{-4}$ |
| 4 | $8.29\times10^{-5}$ | $1.76\times10^{-4}$ |
| 8 | $6.95\times10^{-5}$ | $1.49\times10^{-4}$ |

**Table S3.** Summary of $J_{ph}$-$V_{eff}$ parameters of OSC devices based on (PTzBI-oF + network)/PYIT blend films. The self-healable network was prepared with varying BVTD ratios.

| BVTD ratio (%) | $P_{diss}$ (%) |
|---|---|
| 0 | 96.12 |
| 2 | 94.67 |
| 4 | 92.84 |
| 8 | 90.11 |

**Table S4.** Summary of $1/C^2$-$V$ plot parameters.

| | $N_A$ ($cm^{-3}$) | $V_{bi}$ (V) |
|---|---|---|
| 0% | $1.50\times10^{15}$ | 1.21 |
| 2% | $1.57\times10^{15}$ | 1.08 |
| 4% | $1.65\times10^{15}$ | 0.98 |
| 8% | $1.75\times10^{15}$ | 0.88 |

**Table S5.** Summary of tDOS-$E_\omega$ plot parameters.

| | Peak type | Location ($E_t$) (eV) | Width (σ) |
|---|---|---|---|
| 0% | Gauss | 0.3840 | 0.00836 |
| 2% | Gauss | 0.3806 | 0.00895 |
| 4% | Gauss | 0.3848 | 0.01004 |
| 8% | Gauss | 0.3888 | 0.01131 |

**Table S6**. Summary of the fitting results for GIWAXS *I-q* curves of PTzBI-oF/PYIT, and (PTzBI-oF + network)/PYIT films. The self-healable network was prepared with 4 wt% BVTD relative to PTzBI-oF.

| | IP | | | | |
|---|---|---|---|---|---|
| | Q ($Å^{-1}$) | d-spacing (Å) | FWHM ($Å^{-1}$) | CCL (Å) | Area |
| PTzBI-oF/PYIT | 0.30 | 20.92 | 0.17 | 38.00 | 2.38 |
| (PTzBI-oF + network)/PYIT | 0.30 | 21.08 | 0.15 | 43.91 | 1.96 |
| | OOP | | | | |
| | Q ($Å^{-1}$) | d-spacing (Å) | FWHM ($Å^{-1}$) | CCL (Å) | Area |
| PTzBI-oF/PYIT | 1.72 | 3.70 | 0.36 | 17.67 | 5.99 |
| (PTzBI-oF + network)/PYIT | 1.71 | 3.73 | 0.34 | 18.67 | 5.09 |

**Table S7.** Fitting results of RSoXS I-q curves with correlation length model.

| Thin film | PTzBI-oF/PYIT | (PTzBI-oF + network)/PYIT |
|---|---|---|
| Scale | 6.4928 | 1.1068 |
| Background | 0.00044 | 0.0005 |
| *A* | 1.89E-07 | 6.12E-09 |
| *C* | 0.001563 | 0.015934 |
| *n* | 1.7423 | 2.4854 |
| *m* | 2.7512 | 2.4421 |
| $\xi$ [Å] | 81.68 | 105.15 |

**Table S8.** Mechanical parameters measured from stress-strain curves of PYIT, PTzBI-oF, PTzBI-oF + network, (PTzBI-oF + network)/PYIT films. The self-healable networks were prepared with varying weight ratios of BVTD relative to PTzBI-oF.

| Film | COS (%) | Young's modulus (MPa) |
|---|---|---|
| PYIT | 5.01 | 175.68 |
| PTzBI-oF | 8.89 | 131.04 |
| PTzBI-oF + network (2% BVTD) | 15.59 | 127.35 |
| PTzBI-oF + network (4% BVTD) | 17.56 | 119.58 |
| PTzBI-oF + network (8% BVTD) | 22.41 | 86.42 |
| PTzBI-oF /PYIT | 7.10 | 164.80 |
| (PTzBI-oF + network (2% BVTD))/PYIT | 10.91 | 141.08 |
| (PTzBI-oF + network (4% BVTD))/PYIT | 15.63 | 122.24 |
| (PTzBI-oF + network (8% BVTD))/PYIT | 18.59 | 103.61 |

**Table S9.** *J-V* parameters of IS-OSCs fabricated with (PTzBI-oF + network)/PYIT blend films. The network was prepared with 8 wt% BVTD relative to PTzBI-oF.

| Cycle | Strain | $V_{OC}$ (V) | $J_{SC}$ (mA cm$^{-2}$) | FF (%) | PCE (%) |
|---|---|---|---|---|---|
| 1st | 0% | 0.881 | 23.09 | 46.91 | 9.64 |
| | 10% | 0.872 | 22.76 | 43.86 | 8.78 |
| | 20% | 0.871 | 22.43 | 41.55 | 8.20 |
| | 30% | 0.855 | 22.06 | 40.98 | 7.72 |
| | 40% | 0.852 | 20.78 | 39.73 | 7.03 |
| 2nd | Return to 0% | 0.860 | 22.14 | 42.96 | 8.25 |
| | Return to 0% (after 30 min) | 0.876 | 22.97 | 46.87 | 9.53 |
| | 10% | 0.867 | 22.26 | 44.02 | 8.58 |
| | 20% | 0.861 | 21.64 | 42.97 | 8.08 |
| | 30% | 0.850 | 21.51 | 38.82 | 7.10 |

**Table S10.** Summary of the fitting results for GIWAXS I-q curves of PTzBI-oF + network films under 5% and 15% strains. The self-healable network was prepared with 4 wt% BVTD relative to PTzBI-oF.

| Strain | IP | | | | |
|---|---|---|---|---|---|
| | q ($Å^{-1}$) | d-spacing (Å) | FWHM ($Å^{-1}$) | CCL (Å) | Packing number (CCL/d-spacing) |
| 0% | 0.29 | 21.88 | 0.073 | 85.50 | 3.91 |
| 5%-perp | 0.28 | 22.35 | 0.087 | 72.54 | 3.25 |
| 5%-para | 0.29 | 21.30 | 0.080 | 78.53 | 3.69 |
| 15%-perp | 0.28 | 22.522 | 0.099 | 63.75 | 2.83 |
| 15%-para | 0.29 | 21.42 | 0.080 | 78.04 | 3.64 |

| | OOP | |
|---|---|---|
| | q ($Å^{-1}$) | FWHM ($Å^{-1}$) |
| 0% | 1.73 | 0.25 |
| 5%-perp | 1.74 | 0.25 |
| 5%-para | 1.76 | 0.25 |
| 15%-perp | 1.73 | 0.25 |
| 15%-para | 1.76 | 0.25 |

**Table S11.** Summary of photo-CELIV mobilities of PTzBI-oF/PYIT IS-OSC devices under various strains.

| Device | 0% | 5% | 10% | 15% | 20% |
|---|---|---|---|---|---|
| pristine | 7.51 | 5.84 | 4.07 | 2.60 | 0.31 |
| 8%-BVTD | 6.92 | 5.17 | 4.68 | 4.23 | 3.99 |

**Table S12.** *J-V* parameters of IS-OSCs based on PTzBI-oF/PYIT blend film.

| Cycle | Strain | $V_{OC}$ (V) | $J_{SC}$ (mA cm$^{-2}$) | FF (%) | PCE (%) |
|---|---|---|---|---|---|
| 1st | 0% | 0.885 | 24.93 | 49.01 | 10.88 |
| | 10% | 0.883 | 24.22 | 48.13 | 10.36 |
| | 20% | 0.880 | 23.54 | 46.35 | 9.66 |
| | 30% | 0.881 | 22.74 | 42.86 | 8.64 |
| 2nd | Return to 0% | 0.875 | 22.65 | 43.44 | 8.66 |
| | Return to 0% （after 30 min） | 0.879 | 23.14 | 43.98 | 9.00 |
| | 10% | 0.867 | 20.83 | 42.28 | 7.69 |
| | 20% | 0.795 | 20.56 | 39.80 | 6.54 |
| | 30% | 0.711 | 19.65 | 36.59 | 5.15 |

**Table S13.** Device parameters of IS-OSCs under stretching-releasing cycles of 20% strain in a nitrogen-filled glove box (25 °C, $O_2$ < 5 ppm, $H_2O$ < 0.01 ppm).

| Test cycles | $V_{OC}$ (V) | $J_{SC}$ (mA cm$^{-2}$) | FF (%) | PCE (%) | Norm. PCE (%) |
|---|---|---|---|---|---|
| 0 | 0.885 | 23.03 | 47.92 | 9.83 | 100.00 |
| 50 | 0.883 | 22.52 | 44.54 | 8.96 | 91.15 |
| 100 | 0.876 | 21.56 | 42.00 | 7.93 | 80.67 |
| 150 | 0.855 | 21.01 | 35.71 | 6.41 | 65.20 |
| 200 | 0.846 | 20.23 | 33.41 | 5.72 | 58.18 |

**Table S14.** Device parameters of IS-OSCs under stretching-releasing cycles of 20% strain under ambient conditions (~40% RH, atmospheric oxygen).

| Test cycles | $V_{OC}$ (V) | $J_{SC}$ (mA cm$^{-2}$) | FF (%) | PCE (%) | Norm. PCE (%) |
|---|---|---|---|---|---|
| 0 | 0.884 | 22.65 | 44.03 | 8.82 | 100.00 |
| 50 | 0.878 | 21.84 | 41.71 | 8.00 | 91.27 |
| 100 | 0.854 | 21.02 | 37.29 | 6.70 | 75.96 |
| 150 | 0.828 | 19.58 | 33.40 | 5.41 | 61.34 |
| 200 | 0.811 | 18.86 | 29.95 | 4.58 | 51.93 |

## References:


[1] E. C. Montoto, Y. Cao, K. Hernández-Burgos, C. S. Sevov, M. N. Braten, B. A. Helms, J. S. Moore, J. Rodríguez-López, *Macromolecules* **2018**, *51*, 3539.

[2] Y. Amamoto, H. Otsuka, A. Takahara, K. Matyjaszewski, *Adv. Mater.* **2012**, *24*, 3975.

[3] J. Ilavsky, *J. Appl. Crystallogr.* **2012**, *45*, 324.

[4] X. Luo, G. Freychet, Z. Gan, K. An, H. Du, C. Wang, N. Li, W. Zhong, L. Ying, *Macromolecules* **2023**, *56*, 8928.

[5] T. Lu and F. Chen, *Journal of Computational Chemistry*, 2012, **33**, 580–592.

[6] W. Humphrey, A. Dalke and K. Schulten, *Journal of Molecular Graphics*, 1996, **14**, 33–38.

[7] J. Zhang, Y. Niu, C. Huang, L. Xiao, Z. Chen, K. Yang and Y. Wang, *Polymer Chemistry*, 2012, **3**, 1390-1393.

[8] R. Zheng, Y. Wang, C. Jia, Z. Wan, J. Luo, H. A. Malik, X. Weng, J. Xie and L. Deng, *ACS Appl. Mater. Interfaces*, 2018, **10**, 35533-35538.

[9] Y. Amamoto, H. Otsuka, A. Takahara, K. Matyjaszewski, *Adv. Mater.* **2012**, 24, 3975

[10] N. J. Bongiardina, S. M. Soars, M. Podgorski, C. N. Bowman, *Polymer Chemistry* **2022**, *13*, 3991

[11] P. Wang, L. Yang, B. Dai, Z. Yang, S. Guo, G. Gao, L. Xu, M. Sun, K. Yao and J. Zhu, *Eur. Polym. J.*, 2020, **123**, 109382.

[12] X. Cao, P. Zhang, N. Guo, Y. Tong, Q. Xu, D. Zhou and Z. Feng, *RSC Advances*, 2021, **11**, 2985-2994.